ELSEVIER

Earth and Planetary Science Letters 199 (2002) 473–482

EPSL

www.elsevier.com/locate/epsl

Discordant paleomagnetic direction in Miocene rocks from the central Tarim Basin: evidence for local deformation and inclination shallowing

G. Dupont-Nivet [a,*], Z. Guo [b], R.F. Butler [a], C. Jia [c]

[a] *Department of Geosciences, University of Arizona, Tucson, AZ 85721, USA*
[b] *Department of Geology, Peking University, Beijing 100871, PR China*
[c] *Petrochina Company Limited, Beijing 100011, PR China*

Received 1 November 2001; received in revised form 26 February 2002; accepted 27 February 2002

Abstract

From exposures at the southeastern end of the Maza Tagh range in the central Tarim Basin (latitude: 38.5°N; longitude: 80.5°E), 55 paleomagnetic sites were collected from red mudstones and sandstones of the Miocene Wuqia Formation. Thermal demagnetization revealed a high unblocking temperature characteristic remanent magnetization (ChRM). Five sites collected across a kink fold yield a positive fold test at 99% confidence level. The mean directions computed from normal and reversed polarity sites are antipodal suggesting a primary origin for the ChRM. In stratigraphic coordinates, the final set of 30 site-mean ChRM directions yields a section-mean direction: inclination (I) = 29.4°; declination (D) = 24.7°; α_{95} = 6.2°. When compared to the Miocene expected direction (at 20 Ma), the observed direction indicates 30.8 ± 5.5° flattening of inclination and 15.3 ± 6.7° clockwise vertical-axis rotation. Anisotropy of magnetic susceptibility measurements on 155 samples show a strong foliation of 1.092 with a sub-vertical minimum susceptibility axis. These observations indicate a rock-magnetic (depositional or compaction shallowed) origin for the inclination flattening. The clockwise deflection of the observed declination can be interpreted as either: (1) 15.3 ± 6.7° clockwise rotation of the entire Tarim Basin since the Miocene; or (2) a local km-scale structural deformation. It is not a simple matter to discard the interpretation of 15.3 ± 6.7° clockwise rotation of the Tarim Basin because the fastest rates of rotation determined from global positioning system and slip-rate studies of Quaternary faults could produce such a rotation if extrapolated to 20 Ma. Nevertheless, we argue that local deformation is the preferred interpretation because the map pattern of local structures shows ~20° clockwise deflection toward the southeastern end of the Maza Tagh range where the paleomagnetic samples were collected.

Keywords: paleomagnetism; tectonics; Miocene; sedimentary rocks; Asia

1. Introduction

The Tarim Basin is the largest intracontinental basin in China. This relatively undeformed crustal block within the Indo–Asian collision system is

* Corresponding author. Tel.: +1-520-621-4566; Fax: +1-520-621-2672.
E-mail address: gdn@geo.arizona.edu (G. Dupont-Nivet).

0012-821X/02/$ – see front matter
PII: S0012-821X(02)00566-6

separated from the Tibetan Plateau and Qaidam Basin to the south by the left-lateral Altyn Tagh Fault (Fig. 1a). To the north of the Tarim Basin is the Tien Shan which has experienced Cenozoic compressional deformation. The Tarim Basin is interpreted as a secondary indentor transmitting deformation north from the Himalaya–Tibetan orogen to the Tien Shan and Kazakhstan [1,2]. Therefore determining the Cenozoic kinematics of the Tarim Basin is essential to understanding the Indo–Asian collision [3,4].

An aspect of particular tectonic significance is possible rotation of the Tarim Basin about a nearby Euler pole and the relationship of such rotation to the onset of Tien Shan deformation in the Early Miocene [5–7]. The west to east decrease in width of the Tien Shan has been interpreted to indicate differential north–south shortening resulting from $7 \pm 2.5°$ of clockwise rotation for the Tarim Basin [8]. Kinematic models derived from Quaternary fault slip rates [9,10] have predicted clockwise rotation at a rate of $\sim 0.5°$/Myr. Moreover, the recent global positioning system (GPS) [11,12] and seismic-moment tensor analyses [13], along with neotectonic studies [14], indicate rapid convergence in the Tien Shan which may imply clockwise rotation of the Tarim Basin at a rate approaching 1°/Myr. However, it is difficult to know how far back in geologic time these rotation rates can be extrapolated. In principle, paleomagnetism can allow determination of net rotation back to the age of the rocks analyzed.

Paleomagnetic studies of Cretaceous red sedimentary rocks from the northwestern and northern perimeter of the Tarim Basin [15,16] suggest little net rotation while results from Tertiary sedimentary rocks of the Western Kunlun Shan and adjacent to the Altyn Tagh Fault [17–19] indicate rotations dominated by local structures. Calculated rotations are summarized in Table 1 and illustrated in Fig. 1b. All of these paleomagnetic results are from rocks which are allochtonous to the Tarim Basin. In an attempt to more clearly determine the rotation of the Tarim Basin sensu strictu, we undertook a paleomagnetic study of Miocene red sedimentary rocks from the Maza Tagh range in the central Tarim Basin.

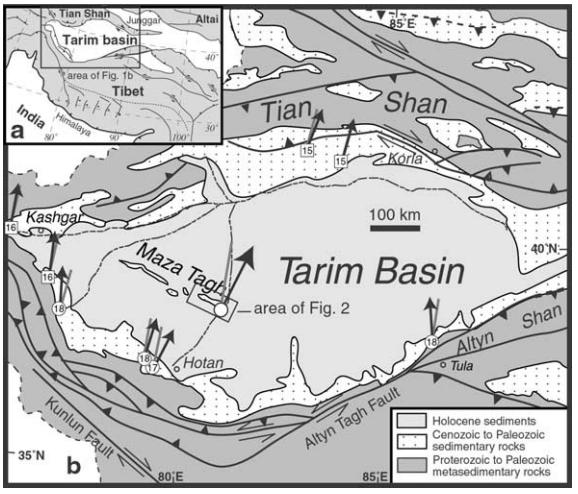

Fig. 1. (a) General tectonic map of the Indo–Asia collision system showing topography over 2000 m (gray) and major structures. (b) Paleomagnetic results from Cretaceous (squares) and Tertiary (circles) rocks of the Tarim Basin region. The observed declinations (black arrows) are compared to the expected declination (gray line) computed from the APWP of Eurasia [29]. Large symbol: this study. Smaller symbols with reference numbers are from previous paleomagnetic studies (results in Table 1).

2. Paleomagnetic sampling and analysis

The Maza Tagh range extends in a northwest–southeast direction for several hundred km with a 300 m relief above the average ~ 1200 m elevation of the Tarim Basin. The fundamental structure is a northeast verging thrust exposing Permian and Late Tertiary rocks [20] (Fig. 2). Following standard procedures [21], 55 sites (site is eight or more samples within one sedimentary horizon) were collected at the southeastern end of the range in a 255 m thick homoclinal section of dark red mudstones and sandstones interbedded with orange cross-bedded coarse sandstone of the Wuqia Formation (N_{1wq1} and N_{1wq2}). A Miocene age for the Wuqia Formation is indicated by fossil assemblages from seven correlated stratigraphic sections within the Maza Tagh range including our sampled section [22]. Other than at the southeastern end of the range, outcrops of the Tertiary strata were inaccessible because of limited incision in this extremely arid environment. At the western end of the investigated

area, five sites were collected from Permian basalts (Fig. 2) but paleomagnetic analyses of these samples indicate remagnetization of indeterminate age and these results are not further discussed.

Samples from five sites were destroyed either during shipment or sample preparation. All prepared samples were stored, thermally demagnetized and measured within a shielded room with average magnetic field intensity under 200 nT. Measurements of natural remanent magnetization (NRM) were done using a three-axis cryogenic magnetometer (2G model 755R). Intensities of NRM ranged from 4×10^{-2} A/m to 1×10^{-3} A/m. Following initial NRM measurements, samples were thermally demagnetized in 10–20 steps from 50°C to 700°C with increments as small as 5°C. After removal of a small present field component below 300°C, demagnetization to higher temperatures was generally successful in isolating a characteristic remanent magnetization (ChRM) as evidenced by a progression of vector end points to the origin of orthogonal projection diagrams (Fig. 3a). For these samples, principal component analysis [23] of NRM at four or more successive temperature steps was used to determine the ChRM. Most samples had a ChRM with high unblocking temperatures in the 650–690°C range and maximum angular deviation determined from principal component analysis was less than 5°. These high unblocking temperatures and isothermal remanent magnetization (IRM) acquired predominantly above 300 mT and still increasing at 1 T (Fig. 3b) suggest that hematite is the carrier of the ChRM. Following determination of at least four sample ChRM directions from a site, site-mean directions were determined using standard statistical methods [24]; sample ChRM directions more than two angular deviations from the preliminary site-mean direction were rejected prior to calculation of the final site-mean direction. From the 50 demagnetized sites, nine sites had less than four sample ChRM directions and were rejected for

Table 1
Paleomagnetic results from the Tarim Basin region

Locality	Age	Location		Observed direction				Reference pole				Rotation	Flattening
		Lat. (°N)	Lon. (°E)	I_m (°)	D_m (°)	α_{95} (°)	n	Lat. (°N)	Lon. (°E)	A_{95} (°)	Age (Ma)	$R\pm\Delta R$ (°)	$F\pm\Delta F$ (°)
Maza Tagh	N_1	38.5	80.5	29.4	24.7	6.2	30	84.1	149.1	2.2	10	16.8 ± 6.2	29.5 ± 5.2
Maza Tagh	N_1	38.5	80.5	29.4	24.7	6.2	30	82.3	147.6	3.3	20	14.6 ± 6.7	30.1 ± 5.5
Jianglisai [18][a]	N_1	38.0	86.5	39.6	358.4	6.7	28	82.3	147.6	3.3	20	−10.6 ± 7.8	20.8 ± 5.8
Aertashi [18][a]	E_3	38.1	76.4	36.9	17.6	5.0	56	81.0	132.8	2.7	30	7.4 ± 5.8	24.6 ± 4.4
Aertashi [17]	E	37.0	79.0	30.0	27.8	13.3	5	80.2	145.4	3.6	40	16.0 ± 12.9	29.5 ± 10.9
Puska [18][a]	E_2	37.1	78.4	24.3	4.3	8.4	22	77.9	149.0	4.3	50	−10.7 ± 8.6	35.1 ± 7.4
Wuqia [16][b]	K_2	39.5	75.0	40.0	11.0	7.4	11	75.7	201.6	3.3	80	−2.3 ± 8.3	9.3 ± 6.6
Yingjisha [16]	K_2	38.5	76.4	37.1	7.6	9.9	6	75.7	201.6	3.3	80	−5.8 ± 10.4	11.4 ± 8.5
Kuche [15][c]	K_2	41.6	83.5	39.2	16.3	8.6	4	75.7	201.6	3.3	80	1.1 ± 9.5	14.6 ± 7.4
Wuqia [16][b]	K_1	39.5	75.0	33.0	11.6	14.0	4	76.3	212.6	5.2	120	1.1 ± 14.2	14.8 ± 12.2
Yingjisha [16]	K_1	38.5	76.4	41.0	14.8	8.9	3	76.3	212.6	5.2	120	4.1 ± 10.6	5.9 ± 8.7
Paicheng [15][c,d]	K_1	41.8	82.0	42.0	22.0	9.0	6	76.3	212.6	5.2	120	9.8 ± 10.9	9.8 ± 8.5

Locality – name of the paleomagnetic sampling locality with references; age – geological age of sampled rocks (K_1 and K_2 – Lower and Upper Cretaceous; E_1, E_2 and E_3 – Lower, Middle and Upper Paleogene; E – undifferentiated Paleogene; N_1 – Miocene); location Lat. and Lon. – latitude and longitude of sampling locality; observed direction I_m, D_m, α_{95} and n – mean inclination, mean declination, radius of the 95% confidence limit and number of sites; reference pole Lat., Lon., A_{95} and age – latitude, longitude, radius of 95% confidence limit and age of the pole used to calculate the expected directions [29]. Rotation (R) – vertical-axis rotation determined by observed declination minus expected declination (positive indicates clockwise rotation); ΔR – 95% confidence limit on rotation; flattening (F) – flattening of inclination indicated by expected inclination minus observed inclination; ΔF – 95% confidence limit on flattening.

[a] Results corrected in [19].

[b] Age of sampled section suggested to be Tertiary by Gilder et al. [38].

[c] Location of these localities corrected from original publication.

[d] May suffer from incomplete structural correction [44].

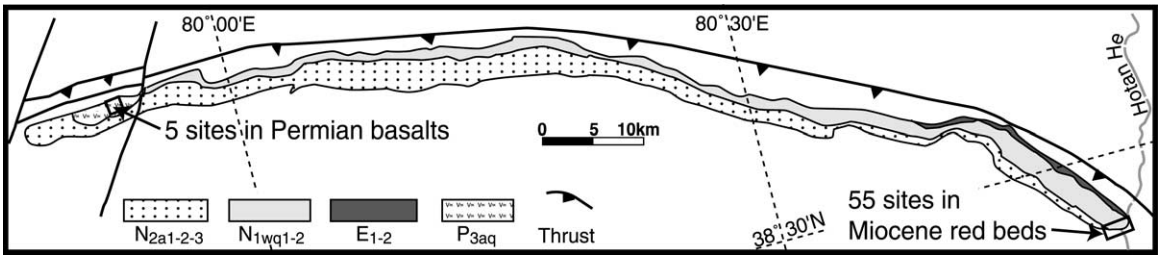

Fig. 2. Geologic map of the eastern Maza Tagh [22]. Sampled section at the eastern tip of the structure is red beds of the upper and lower member Miocene (N_1 in Chinese terminology) Wuqia Formation (N_{1wq1-2}). N_{1wq1-2} is conformable on top of Paleocene–Eocene (E_{1-2}) gypsum rich formation and underlies Pliocene (N_2) formation of mudstone and sandstone interlayered with poorly consolidated conglomerates. At the western end, outcrops of Permian basalts (P_3) were sampled.

further analysis. Site-mean directions were calculated from the remaining 41 sites. Seven sites corresponding to parts of the section affected by fractures associated with meter-scale deformation had a confidence limit (α_{95}) larger than 20° and were rejected from further analysis. Finally, from the 55 sites collected, 34 site-mean ChRM directions were determined. These site-mean directions are listed in Table 2 and illustrated in Fig. 3c. Normal and reversed polarity groups of directions are immediately apparent with the exception of four sites with aberrant WNW declinations (see crossed directions on Fig. 3c and sites indicated by * in Table 2). These site-mean directions deviate in declination from the cluster of reversed polarity directions suggesting that these beds were affected by small-scale rotation (slumping?) about an axis perpendicular to bedding. These directions were discarded prior to calculating the mean direction from the sampled section. For the remaining 30 site-mean directions, the between-site dispersion of normal polarity site-mean directions

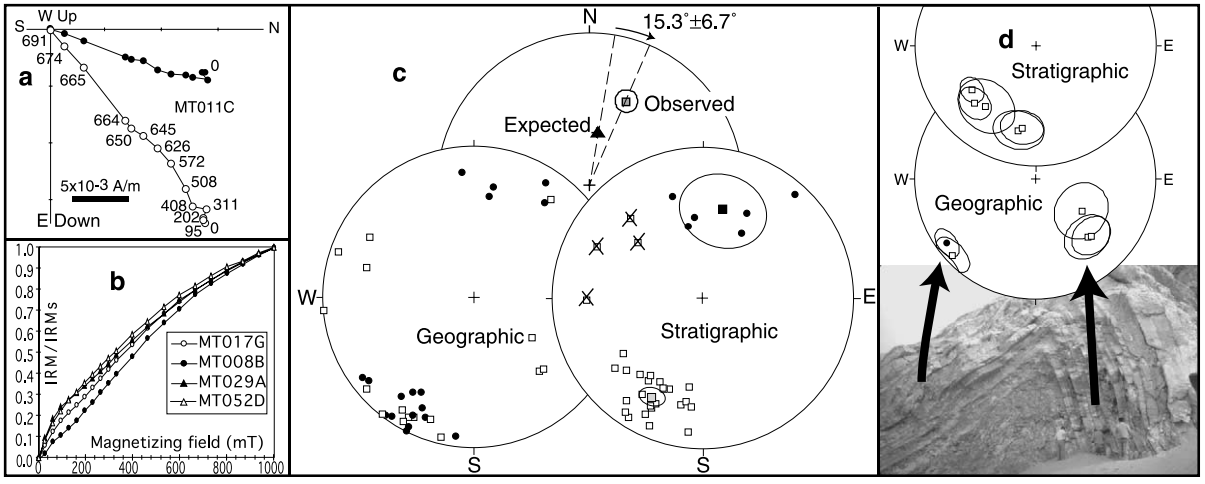

Fig. 3. (a) Vector end point diagram of representative sample (MT011C). (b) IRM acquisition behaviors of typical samples. (c) Two bottom equal-area projections show site-mean directions projected on the lower hemisphere (black symbols) and upper hemisphere (open symbols) in geographic and stratigraphic coordinates. In stratigraphic coordinates, the mean of normal sites is shown by a black square and the mean of reverse polarity sites is shown by a gray square; surrounding ovals are 95% confidence limits. Crossed symbols are site-mean directions discarded from calculation of the final mean direction. In the top diagram, the observed mean direction is shown by a gray square with 95% confidence limit and the expected direction computed from the APWP of Eurasia at 20 Ma [29] is shown by a black triangle. (d) Fold test was performed across this kink fold within the otherwise homoclinal sampled section. Equal-area projections show in situ and tilt-corrected site-mean directions with 95% confidence circles.

(precision parameter $k_n = 10.3$) is significantly larger than that for reversed polarity sites ($k_r = 27.5$). Thus the reversal test [25] cannot be formally applied to this collection of site-mean directions. Nevertheless the mean of the normal polarity sites is indistinguishable from the antipode of the mean for the reverse polarity sites. A kink fold within the sampled section allowed a fold test of the site-mean ChRM directions from five of the six sites collected across this fold (Fig. 3d). These site-mean directions (sites MT020, 21, 22, 24, 25; Table 2) yield a positive

Table 2
Site-mean ChRM directions of the Wuqia Formation

Site	*P*	Height (m)	Fm.	Geographic		Stratigraphic		α_{95} (°)	*n*/*N*	*k*	Dip (°)	Dip az. (°)
				I (°)	*D* (°)	*I* (°)	*D* (°)					
MT029	R	240	N_{1wq2}	−9.9	208.2	−34.6	203.0	14.7	8/8	13.3	27.5	232.3
MT028	R	230	N_{1wq2}	0.3	206.6	−24.2	203.9	4.6	8/8	126.6	27.5	232.3
MT027	R	220	N_{1wq2}	15.0	201.9	−8.9	202.7	13.3	5/5	27.4	27.5	232.3
MT026	R	210	N_{1wq2}	−11.9	206.5	−36.1	200.4	6.9	7/8	79.0	27.5	232.3
MT016	R	198	N_{1wq2}	7.5	187.1	−11.9	186.3	11.9	8/8	19.8	27.5	232.3
MT014	R	196.5	N_{1wq2}	4.1	206.7	−20.6	204.9	5.2	8/8	102.0	27.5	232.3
MT013	R	196	N_{1wq2}	−12.1	212.1	−37.6	207.2	6.5	8/8	74.0	27.5	232.3
MT011	N	197	N_{1wq2}	22.6	37.0	48.8	30.7	8.8	8/8	35.8	27.5	232.3
MT010	N	196.5	N_{1wq2}	11.4	32.1	36.9	27.3	8.5	8/8	37.8	27.5	232.3
MT009	N	196	N_{1wq2}	27.1	10.3	45.2	354.2	12.4	7/8	21.2	27.5	232.3
MT008	N	195.5	N_{1wq2}	33.2	8.8	50.0	348.7	9.2	8/8	32.3	27.5	232.3
MT007	N	193.5	N_{1wq2}	17.8	354.7	30.4	343.4	10.2	8/8	26.7	27.5	232.3
MT005	N	192	N_{1wq1}	−18.6	38.4	8.7	41.7	13.7	8/8	15.1	27.5	232.3
MT057*	R		N_{1wq1}	−27.7	285.2	−42.8	310.6	8.9	6/6	47.9	37.3	230.5
MT055*	R		N_{1wq1}	−21.6	299.8	−29.5	318.0	12.6	7/8	24.5	37.3	230.5
MT053	R		N_{1wq1}	26.1	212.7	−9.3	214.3	5.1	7/8	146.5	37.3	230.5
MT051	R		N_{1wq1}	−1.7	217.7	−37.9	214.2	15.8	7/8	13.3	37.3	230.5
MT050	R		N_{1wq1}	12.5	207.1	−21.7	205.8	5.8	6/6	111.1	37.3	230.5
MT049	R		N_{1wq1}	19.6	216.3	−16.4	216.6	6.2	6/8	123.7	37.3	230.5
MT025	R	80	N_{1wq1}	−7.0	229.2	−30.8	226.3	10.7	8/8	24.3	24.0	233.0
MT024	R		N_{1wq1}	10.1	233.8	−35.7	234.9	8.3	8/8	40.3	46.0	229.0
MT023*	R		N_{1wq1}	−0.1	264.7	−24.1	269.1	10.9	6/8	32.3	31.0	227.0
MT022	R		N_{1wq1}	−33.5	135.7	−31.1	189.3	12.9	8/8	17.0	71.0	71.0
MT021	R		N_{1wq1}	−34.8	138.4	−28.5	191.4	15.0	8/8	12.8	72.0	71.0
MT020	R	70	N_{1wq1}	−51.0	125.0	−34.7	219.1	18.6	8/8	8.6	77.0	75.0
MT043	R		N_{1wq1}	20.1	205.0	−14.8	206.2	5.7	8/8	83.9	38.5	232.2
MT042	R		N_{1wq1}	2.3	216.7	−34.6	213.3	11.5	8/8	21.2	38.5	232.2
MT041	R		N_{1wq1}	11.9	231.4	−26.6	231.3	13.7	8/8	15.1	38.5	232.2
MT040	R		N_{1wq1}	28.7	209.0	−7.3	211.8	9.9	7/7	32.5	38.5	232.2
MT039	R	30	N_{1wq1}	4.9	214.3	−25.2	212.4	9.2	8/8	32.5	31.8	232.6
MT038*	R		N_{1wq1}	−6.3	288.3	−22.9	295.6	5.0	8/8	107.7	31.8	232.6
MT037	R		N_{1wq1}	−5.0	192.9	−28.5	186.2	9.7	8/8	33.7	31.8	232.6
MT036	R		N_{1wq1}	−6.2	209.3	−35.0	203.9	11.1	8/8	26.4	31.8	232.6
MT035	R	0	N_{1wq1}	−14.7	199.2	−39.9	188.7	12.7	6/8	23.9	31.8	232.6
Mean	Geographic			4.1	23.7			10.4	30/34	7.3		
	Stratigraphic					29.4	24.7	6.2	30/34	19.7		

P is the polarity indicated by N for normal and R for reverse; height is the stratigraphic height in the sampled section; Fm. is the name of the sampled formation; *I* and *D* are inclination and declination of site-mean directions in geographic and stratigraphic coordinates; α_{95} is the radius of the 95% confidence limit on the site-mean direction; *n*/*N*: *n* is the number of ChRM directions used to calculate the site-mean and *N* the number of demagnetized samples; *k* is the concentration factor; Dip and Dip az. are the mean dip and dip azimuth of bedding in different parts of the section. Last line indicates mean direction for the section calculated from all sites except outliers marked with an asterisk.

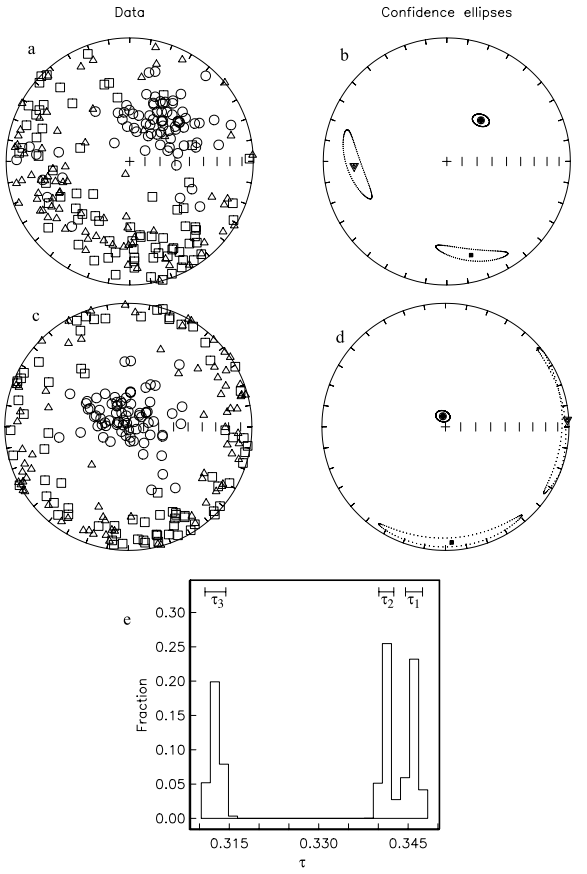

Fig. 4. AMS data. (a) Lower hemisphere projection of directions of maximum (squares), intermediate (triangles), and minimum (circles) eigenvectors in geographic coordinates. (b) Lower hemisphere projection of the mean eigenvectors with bootstrap 95% confidence ellipses. (c and d) Same as a and b in stratigraphic coordinates. (e) Histogram of eigenvalues associated to eigenvectors plotted in c (τ_1: maximum; τ_2: intermediate; τ_3: minimum). The bounds containing 95% of each eigenvalue are shown above the histogram.

fold test [26] at the 99% confidence level (precision parameter k and test statistic ξ of $k_g = 2.4$ and $\xi_g = 4.6$ in geographic coordinates versus $k_s = 20.3$ and $\xi_s = 0.621$ in stratigraphic coordinates; 99% critical value at $\xi = 3.6$; minimum ξ value was obtained at 100% unfolding) indicating a pre-folding origin for the characteristic magnetization. Taken together, the positive fold test, high-temperature ChRM stability, and precise determination of sample ChRM directions suggest a primary origin for the characteristic magnetization.

The final set of 30 site-mean ChRM directions is used to compute a mean direction for the sampled Miocene sedimentary rocks of the Maza Tagh. In normal polarity format and stratigraphic coordinates, the section-mean direction has inclination (I) = 29.4°, declination (D) = 24.7°, with 95% confidence limit (α_{95}) = 6.2°. This mean direction can be compared to the Miocene expected direction at the sampling location using methods described by Beck [27] and Demarest [28]. Because of the age uncertainty and/or age interval of the sampled Miocene rocks, we compare the section-mean direction to the expected direction computed from both the 10 Ma and 20 Ma reference paleomagnetic poles for Eurasia [29]. Using these reference poles, comparison of the section-mean direction to these expected directions indicates respectively $30.2 \pm 5.2°$ and $30.8 \pm 5.5°$ flattening of inclination and $17.5 \pm 6.1°$ and $15.3 \pm 6.7°$ clockwise vertical-axis rotation (Table 1).

Of the 226 core samples from the 30 sites with interpretable site-mean directions, 169 samples from sandstones and mudstones were long enough to allow preparation of a second specimen for measurements of anisotropy of magnetic susceptibility (AMS). These measurements were made using a Sapphire Instruments magnetic susceptibility bridge (model SI-2). The bulk susceptibility ranges from 9.41×10^{-5} to 4.34×10^{-4} SI with a mean of 2.51×10^{-4} SI. The mean directions of principal susceptibility axes were determined using bootstrap statistical methods [30]. After rejecting results from 14 specimens that yielded susceptibility axes more than two angular standard deviations from the preliminary mean directions, AMS results from 155 specimens were used to calculate the mean principal susceptibility axes directions shown in Fig. 4a–d. The minimum axis eigenvalues (τ_3) plotted on the histogram (Fig. 4e) are clearly distinct from the intermediate and maximum axis eigenvalues (τ_1 and τ_2). This indicates an oblate AMS ellipsoid [30] which is confirmed by the value of the shape parameter $T = 0.75$ [31]. Upon restoring the beds to horizontal, minimum axes cluster in a sub-vertical ($I = 83.1°$, $D = 325.3°$) direction while intermediate and maximum axes are broadly distributed in the horizontal plane. Thus the AMS fabric is quite

clearly related to deposition or compaction. Clustering of the minimum susceptibility axes near vertical following restoration of bedding to horizontal is especially dramatic for the samples collected in the kink fold, indicating that the fabric was acquired prior to deformation.

The magnitude of the susceptibility anisotropy for the Miocene sedimentary rocks of the Maza Tagh expressed by percent anisotropy [32] is 3.298% while the total anisotropy is 0.099 [33]. The AMS foliation ($P_3 = \tau_2/\tau_3 = 1.092$ [34]) is larger than foliation observed from Early Cretaceous Kapushaliang red beds ($P_3 = 1.035$) of the northern Tarim Basin [35]. This is an important result because detailed rock-magnetic analyses by Tan [35] have shown that the inclination of ChRM in the Kapushaliang red beds has undergone 20–30° inclination shallowing either due to particle shallowing during deposition or post-depositional compaction. The larger AMS foliation observed for the Miocene sedimentary rocks of the Maza Tagh strongly suggests that the $\sim 30°$ flattening of ChRM inclination in these rocks is dominantly or entirely a rock-magnetic effect.

3. Discussion and conclusions

The $15.3 \pm 6.7°$ clockwise deflection of the Maza Tagh observed declination from the expected declination requires either a local structural or regional tectonic explanation. Two alternative explanations are immediately apparent: (1) the entire Tarim Basin, including the Maza Tagh range, experienced $15.3 \pm 6.7°$ clockwise rotation since the Miocene; or (2) local km-scale structural deformation affected the sampled section, deflecting the observed paleomagnetic declination from the expected declination. Although we strongly favor a local deformation as the preferred interpretation, it is not a simple matter to dismiss a $15.3 \pm 6.7°$ clockwise rotation of the entire Tarim Basin over the past ~ 20 Myr as an outrageous hypothesis.

Arguments for clockwise rotation of the entire Tarim Basin have been advanced based on evidence from structural geology [8], Quaternary fault slip rates [9,10], GPS observations [11,12], and seismic-moment tensor analyses [13]. So the question is not whether the Tarim Basin has experienced clockwise rotation, but rather over what time interval that rotation has occurred and how large has been the total rotation? The Quaternary fault slip rate and GPS observations indicate clockwise rotation at short-term rates of 0.5°/Myr to perhaps 1°/Myr. Extrapolation of these short-term rates over the past 15–20 Myr could produce the $15.3 \pm 6.7°$ clockwise rotation of the observed paleomagnetic direction from the Maza Tagh range. On the other hand, geologic evidence indicates a smaller clockwise rotation of $7 \pm 2.5°$ for the Tarim Basin since the onset of Tien Shan deformation in the Early Miocene [5,6,8]. Also rotation of the Tarim Basin implies rotation of the Altyn Tagh Fault which separates it from the Qaidam Basin on its southern margin. In turn, rotation of the Altyn Tagh Fault would require rotation of the Qaidam Basin. However, paleomagnetic observations from Miocene and Oligocene rocks from the interior of the Qaidam Basin limit rotation to $\leq 5°$ over the past 30 Myr [36]. Thus while the highest estimated short-term rates of rotation for the Tarim Basin could permit $15.3 \pm 6.7°$ clockwise rotation if extrapolated for 15–20 Myr, estimates of net rotation over the past 20 Myr based on paleomagnetic and regional geologic constraints favor smaller rotation.

An argument for local deformation of the sampled Maza Tagh section accounting for the $15.3 \pm 6.7°$ clockwise deflection of the observed paleomagnetic declination can be made by inspection of the geologic map of the sampling location (Fig. 2). In map view, the thrust fault that transported the sampled Miocene section to the northeast deflects clockwise near its southeastern terminus where the paleomagnetic samples were collected. Although direct measures of displacement on this thrust fault are not available, the bow shape of the fault trace in map view can reasonably be accounted for by decrease in fault offset from the central part of the Maza Tagh toward the southeastern termination of the fault. As illustrated in Fig. 2, the deflection of the eastern portion of this thrust fault from the regional trend is $\sim 20°$ in a clockwise direction. Thus the regional geologic evidence is consistent with local

km-scale clockwise vertical-axis rotation of the sampled Maza Tagh section as the cause of the $15.3 \pm 6.7°$ clockwise deflection of the observed paleomagnetic declination. Although a combination of regional and local rotations is conceivable, based on the principle that local geologic explanations should be exhausted before paleomagnetic observations are interpreted to require more dramatic regional deformations, we favor the interpretation that the $15.3 \pm 6.7°$ clockwise deflection of the observed declination from the Miocene rocks of the Maza Tagh is due to a local deformation.

Discordant shallow inclinations have been observed in many paleomagnetic studies of Cretaceous to Tertiary red sedimentary rocks in Asia [37] (Table 1). Interpretation of this inclination flattening is not straightforward [38] and tectonic, geomagnetic, and rock-magnetic explanations have been advanced [37–40]. Interpreting the $\sim 30°$ flattening of inclination from the Miocene rocks of the Maza Tagh as the result of northward tectonic displacement would imply ~ 1600 km of intracontinental shortening between the Tarim Basin and Kazakhstan/Siberia since the Miocene. This amount of crustal shortening exceeds geological estimates by about a factor of 10 and the implied rate of displacement for the Tarim Basin exceeds lithospheric plate speeds by more than a factor of 10. Cogné et al. [40] have suggested that tectonic displacements between Siberia and Europe with resulting inaccurate Eurasian reference paleomagnetic poles for central Asia may provide an explanation for the shallow paleomagnetic inclinations. However, motion between Siberia and Europe would have to have occurred during the Neogene to account for shallowed inclinations observed in the Tertiary rocks [41]. No such displacements are evident in the geologic record and it is unlikely that such a young deformation could be missed.

Si and Van der Voo [41] and previous workers [37,39] have argued that persistent non-dipole components of the geomagnetic field could explain the anomalous shallow inclinations observed across central Asia. Although based on scarce Asian paleomagnetic data with few results from igneous rocks, the non-dipole explanation does have the attraction of explaining the pattern of increasingly shallow paleomagnetic inclinations from Europe to Eastern Asia [37,41]. However, there are difficulties with the non-dipole explanation as well. Flattening of paleomagnetic inclinations ranging from 20° to 30° have been observed from Early Cretaceous [35] and Late Jurassic [42] as well as in very young red sedimentary rocks (3.7 Ma Yushu formation in northern Tibet [40] and Youshashan formation [36] in the Qaidam Basin). Thus if non-dipole components of the geomagnetic field are to provide the explanation for the shallow paleomagnetic inclinations from central Asia, this non-dipolar behavior must be very long-lived. In addition, concordant paleomagnetic inclinations observed in Paleogene basalts from the nearby Tien Shan [43] indicate a dipolar configuration of the geomagnetic field during the Tertiary.

The magnitude and orientation of AMS observed for the Miocene sedimentary rocks of the Maza Tagh indicate a strong magnetic foliation in these rocks. This AMS exceeds that observed for the Early Cretaceous Kapushaliang red sedimentary rocks of the northern Tarim Basin from which rock-magnetic data indicate 20–30° shallowing of paleomagnetic inclination by depositional or compaction processes [35]. Our preferred interpretation is that the $\sim 30°$ shallowing of paleomagnetic inclination observed for the Miocene strata of the Maza Tagh is dominantly or entirely a rock-magnetic effect of depositional or compaction processes.

Our interpretations of the discordant paleomagnetic direction from the Miocene red sedimentary rocks of the Maza Tagh are unsatisfying in the sense that we sought paleomagnetic data with clear implications for large-scale tectonics of the Indo–Asian collision. Instead we conclude that local deformation of the sampled section and depositional or compaction shallowing are most likely responsible for the discordant direction. We present our results and interpretations with the intent that others will be inspired to undertake additional studies in other areas of the Tarim Basin that will reveal the Tertiary vertical-axis rotational history of the basin and resolve the origin of shallow paleomagnetic inclinations observed in central Asia.

Acknowledgements

This research was funded by the Continental Dynamics Program of the U.S. National Science Foundation. We thank the Chinese National Petroleum Company (CNPC) for providing major logistical support for the field work without which this project could not have been undertaken. Bill Hart and Lucas Murray provided valuable laboratory assistance. We thank An Yin and Ken Kodama for useful discussions and Rob Van der Voo for alerting us to his work with Jingwei Si on a geomagnetic explanation for shallow paleomagnetic inclinations in central Asia. Careful reviews by Yan Chen, Stuart Gilder, Nadir Halim and an anonymous reviewer helped to improve the manuscript. *[RV]*

References

[1] P. Molnar, P. Tapponnier, Active tectonics of Tibet, J. Geophys. Res. 83 (1978) 5361–5375.
[2] E.A. Neil, G.A. Houseman, Geodynamics of the Tarim basin and the Tian Shan in central Asia, Tectonics 16 (1997) 571–584.
[3] P. Tapponnier, G. Peltzer, A.Y. LeDain, R. Armijo, Propagating extrusion tectonics in Asia: new insights from simple experiments with plasticine, Geology 10 (1982) 611–616.
[4] G. Houseman, P. England, Finite strain calculations of continental deformation I. Method and general results from convergent zones, J. Geophys. Res. 91 (1986) 3651–3663.
[5] A. Yin, S. Nie, P. Craig, T.M. Harrison, F.J. Ryerson, X. Qian, G. Yang, Late Cenozoic tectonic evolution of the southern Chinese Tian Shan, Tectonics 17 (1998) 1–27.
[6] E.R. Sobel, T.A. Dumitru, Thrusting and exhumation around the margins of the western Tarim basin during the India–Asia collision, J. Geophys. Res. 102 (1997) 5043–5063.
[7] B.C. Burchfiel, E.T. Brown, Q. Deng, X. Feng, J. Li, P. Molnar, J. Shi, Z. Wu, H. You, Crustal shortening on the margins of the Tien Shan, Xinjiang, China, Int. Geol. Rev. 41 (1999) 665–700.
[8] J.P. Avouac, P. Tapponnier, M. Bai, H. You, G. Wang, Active thrusting and folding along the northern Tien Shan and Late Cenozoic rotation of the Tarim relative to Dzungaria and Kazakhstan, J. Geophys. Res. 98 (1993) 6755–6804.
[9] G. Peltzer, F. Saucier, Present-day kinematics of Asia derived from geologic fault rates, J. Geophys. Res. 101 (1996) 27943–27956.
[10] J.P. Avouac, P. Tapponnier, Kinematic model of active deformation in central Asia, Geophys. Res. Lett. 20 (1993) 895–898.
[11] K. Abdrakhmatov, S.A. Aldazhanov, B.H. Hager, M.W. Hamburger, T.A. Herring, K.B. Kalabaev, V.I. Makarov, P. Molnar, S.V. Panasyuk, M.T. Prilepin, R.E. Reilinger, I.S. Sadybakasov, B.J. Souder, Y.A. Trapeznikov, V.Y. Tsurkov, A.V. Zubovich, Relatively recent construction of the Tien Shan inferred from GPS measurements of present day crustal deformation rates, Nature 384 (1996) 450–453.
[12] R. Bendick, R. Bilham, J. Freymueller, K. Larson, G. Yin, Geodetic evidence for a low slip rate in the Altyn Tagh fault system, Nature 404 (2000) 69–72.
[13] P. Molnar, S. Ghose, Seismic moments of major earthquakes and the rate of shortening across the Tien Shan, Geophys. Res. Lett. 27 (2000) 2377–2380.
[14] R. Arrowsmith, M.R. Strecker, Seismotectonic range-front segmentation and mountain-belt growth in the Pamir-Alai region, Kyrgyzstan (India–Eurasia collision zone), GSA Bull. 111 (1999) 1665–1683.
[15] Y. Li, Z. Zhang, M. McWilliams, R. Sharps, Y. Zhai, Y. Li, Q. Li, A. Cox, Mesozoic paleomagnetic results of the Tarim craton: Tertiary relative motion between China and Siberia?, Geophys. Res. Lett. 15 (1988) 217–220.
[16] Y. Chen, J.-P. Cogné, V. Courtillot, New Cretaceous paleomagnetic results from the Tarim basin, northwestern China, Earth Planet. Sci. Lett. 114 (1992) 17–38.
[17] S. Gilder, X. Zhao, R. Coe, Z. Meng, V. Courtillot, J. Besse, Paleomagnetism and tectonics of the southern Tarim Basin, northwestern China, J. Geophys. Res. 101 (1996) 22015–22031.
[18] P.E. Rumelhart, A. Yin, E. Cowgill, R.F. Butler, Q. Zhang, X.-F. Wang, Cenozoic vertical-axis rotation of the Altyn Tagh fault system, Geology 27 (1999) 819–822.
[19] A. Yin, Correction Cenozoic vertical-axis rotation of the Altyn Tagh fault system, Geology 28 (2000) 480.
[20] C. Jia, G. Wei, L. Wang, D. Jia, Z. Guo, Tectonic Characteristics and Petroleum, Tarim Basin, China, Petroleum Industry Press, Beijing, 1997, p. 295.
[21] R.F. Butler, Paleomagnetism: Magnetic Domains to Geologic Terranes, Blackwell Scientific Publications, Boston, MA, 1992, pp. 83–104.
[22] R. Zhong, C.J. Wu, H.R. Zhong, B. Li, Field survey report in the Maza Tagh area: southern margin of the Bachu uplift of the Tarim Basin, Tarim Petroleum Exploration Company, 1995, p. 116 (in Chinese).
[23] J.L. Kirschvink, The least-square line and plane and the analysis of paleomagnetic data, Geophys. J. R. Astron. Soc. 62 (1980) 699–718.
[24] R.A. Fisher, Dispersion on a sphere, Proc. R. Soc. Lond. A 217 (1953) 295–305.
[25] P.L. McFadden, M.W. McElhinny, Classification of the reversal test in palaeomagnetism, Geophys. J. Int. 103 (1990) 725–729.

[26] P.L. McFadden, A new fold test for palaeomagnetic studies, Geophys. J. Int. 103 (1990) 163–169.
[27] M.E. Beck, Paleomagnetic record of plate-margin tectonic processes along the western edge of North America, J. Geophys. Res. 85 (1980) 7115–7131.
[28] H.H. Demarest, Error analysis of the determination of tectonic rotations from paleomagnetic data, J. Geophys. Res. 88 (1983) 4321–4328.
[29] R.J. Enkin, Z. Yang, Y. Chen, V. Courtillot, Paleomagnetic constraints on the geodynamic history of the major blocks of China from the Permian to the present, J. Geophys. Res. 97 (1992) 13953–13989.
[30] L. Tauxe, Paleomagnetic Principles and Practice, Kluwer Academic Publisher, Dordrecht, 1998, 299 pp.
[31] Jelinek, 1981#V. Jelinek, Characterization of the magnetic fabric of rocks, Tectonophysics 79 (1981) T63–T67.
[32] C. Constable, L. Tauxe, The bootstrap for magnetic susceptibility tensors, J. Geophys. Res. 95 (1990) 8383–8395.
[33] W. Owens, Mathematical model studies on factors affecting the magnetic anisotropy of deformed rocks, Tectonophysics 24 (1974) 115–131.
[34] F. Stacey, G. Joplin, J. Lindsay, Magnetic anisotropy and fabric of some foliated rocks from S.E. Australia, Geophys. Pur. Apll. 47 (1960) 30–40.
[35] X. Tan, Correcting the bias toward shallow paleomagnetic inclinations in hematite-bearing sedimentary rocks: Theory, experiments, and applications, Ph.D. thesis, Lehigh University, 2001.
[36] G. Dupont-Nivet, R.F. Butler, A. Yin, X. Chen, Paleomagnetism indicates no Neogene rotation of the Qaidam Basin in North Tibet during Indo–Asian Collision, Geology (2002), in press.
[37] A. Chauvin, H. Perroud, M.L. Bazhenov, Anomalous low palaeomagnetic inclinations from Oligocene–Lower Miocene red beds of the south-west Tien Shan, Central Asia, Geophys. J. Int. 126 (1996) 303–313.
[38] S. Gilder, Y. Chen, S. Sen, Oligo–Miocene magnetostratigraphy and rock magnetism of the Xishuigou section, Subei (Gansu Province, western China) and implications for shallow inclinations in central Asia, J. Geophys. Res. 106 (2001) 30505–30522.
[39] M. Westphal, Did a large departure from the geocentric axial dipole hypothesis occur during the Eocene? Evidence from the magnetic polar wander path of Eurasia, Earth Planet. Sci. Lett. 117 (1993) 15–28.
[40] J.P. Cogné, N. Halim, Y. Chen, V. Courtillot, Resolving the problem of shallow magnetizations of Tertiary age in Asia: Insights from paleomagnetic data from the Qiangtang, Kunlun, and Qaidam blocks (Tibet, China), and a new hypothesis, J. Geophys. Res. 104 (1999) 17715–17734.
[41] J. Si, R. Van der Voo, Too-low magnetic inclinations in central Asia: an indication of a long-term Tertiary non-dipole field?, Terra Nova, in press.
[42] G. Dupont-Nivet, R.F. Butler, A. Yin, D. Robinson, Y. Zhang, W.S. Qiao, Paleomagnetism on arcuate structures along the Altyn Tagh fault: implications for the intracontinental deformation processes in Asia, EOS Trans. AGU 82 (2001), Abstract T12F-06.
[43] M.L. Bazhenov, A.V. Mickolaichuck, Paleomagnetism of Paleogene basalts from the Tien Shan, Kyrgyzstan: rigid Eurasia and dipole geomagnetic field, Earth Planet. Sci. Lett. 195 (2002) 155–166.
[44] Y. Chen, J.-P. Cogne, V. Courtillot, J.-P. Avouac, P. Tapponnier, E. Buffetaut, G.-Q. Wagn, M.-X. Bai, H.-Z. You, M. Li, C.-S. Wei, Paleomagnetic study of Mesozoic continental sediments along the northern Tien Shan (China) and heterogeneous strain in central Asia, J. Geophys. Res. 96 (1991) 4065–4082.